Potent antiviral effect of protoporphyrin IX and verteporfin on SARS-CoV-2 infection

Chenjian Gu[1*], Yang Wu[1*], Huimin Guo[1*], Yuanfei Zhu[1], Wei Xu[1], Yuyan Wang[1], Zhiping Sun[2], Xia Cai[2], Yutang Li[1], Jing Liu[1], Zhenghong Yuan[1], Rong Zhang[1], Qiang Deng[1**], Di Qu[1, 2**], Youhua Xie[1,3**]

[1] Key Laboratory of Medical Molecular Virology (MOE/NHC/CAMS), Department of Medical Microbiology and Parasitology, School of Basic Medical Sciences, Shanghai Medical College, Fudan University

[2] BSL-3 laboratory of Fudan University, School of Basic Medical Sciences, Shanghai Medical College, Fudan University

[3] Children's hospital, Shanghai Medical College, Fudan University

* These authors contribute equally

** Corresponding authors, Youhua Xie, Key Laboratory of Medical Molecular Virology (MOE/NHC/CAMS), School of Basic Medical Sciences, Shanghai Medical College, Fudan University, e-mail, yhxie@fudan.edu.cn; Di Qu, BSL-3 laboratory of Fudan University, School of Basic Medical Sciences, Shanghai Medical College, Fudan University. e-mail, dqu@shmu.edu.cn; Qiang Deng, Key Laboratory of Medical Molecular Virology (MOE/NHC/CAMS), School of Basic Medical Sciences, Shanghai Medical College, Fudan University, e-mail, qdeng@fudan.edu.cn.

ABSTRACT

The infection of SARS-CoV-2 has spread to more than 200 countries and regions and the numbers of infected people and deaths worldwide are expected to continue to rise. Current treatment of COVID-19 is limited and mostly supportive. At present, there is no specific therapeutics against SARS-CoV-2. In this study, we discovered that protoporphyrin IX and verteporfin, two FDA-approved drugs for treatment of human diseases, had significant antiviral effect against SARS-CoV-2, with EC50 values for the reduction of viral RNA at nanomolar concentrations. Both drugs completely inhibited the cytopathic effect (CPE) produced by SARS-CoV-2 infection at lower drug concentrations than that of remdesivir. The selection indices of protoporphyrin IX and verteporfin are 952.74 and 368.93, respectively, suggesting wide safety margins. Both drugs were able to prevent SARS-CoV-2 infection as well as suppress established SARS-CoV-2 infection. The compounds share a porphyrin ring structure. Molecular docking indicates that the compounds may interact with viral receptor ACE2 and could block the cell-cell fusion mediated by ACE2 and viral S protein. Our finding suggests that protoporphyrin IX and verteporfin might be potential antivirals against SARS-CoV-2 infection and also sheds new light on the development of a novel class of small compounds against SARS-CoV-2.

INTRODUCTION

The infection of SARS-CoV-2 (Severe Acute Respiratory Syndrome Coronavirus 2) has spread to more than 200 countries and regions since December 2019. As of April 24, 2020, there are nearly 2.7 million confirmed cases globally, of which more than 190,000 died. Although the development of the pandemic has been contained or alleviated in some countries, the numbers of infected people and deaths worldwide are expected to continue to rise.

SARS-CoV-2 is transmitted through respiratory droplets and close contact, which causes mainly upper and lower respiratory diseases. The majority of infected healthy

adults and children only show mild symptoms including cough, fever, fatigue and diarrhea but the elderly with various chronic diseases are at high risk of development of serious diseases including pneumonia, acute respiratory distress, multiple organ failure and shock. At present, the main treatment of Corona Virus Disease 2019 (COVID-19) is supportive, including non-specific antivirals and symptom-alleviating therapies. Ventilations and intensive care are required for severe cases, calling for early intervention to prevent symptoms from deteriorating.

At present, there is no specific therapeutics against SARS-CoV-2. An earlier case report demonstrated the potential effectiveness of remdesivir in the experimental treatment of an American COVID-19 patient [1]. *In vitro* experiment showed that remdesivir effectively inhibited SARS-CoV-2 replication [2]. The recent data on the compassionate use of remdesivir for patients with severe COVID-19 indicated that clinical improvement was observed in 36 of 53 patients (68%) [3]. Several drugs in clinical use for other diseases have been tested *in vitro* for inhibition of SARS-CoV-2 infection and some of them are in clinical trial [4-8]. Among them, chloroquine and its derivative hydroxychloroquine have drawn intensive debate [9]. Chloroquine and hydroxychloroquine have been shown to inhibit SARS-CoV-2 infection *in vitro* [10] while the clinical trials of hydroxychloroquine reported controversial results [11, 12]. Traditional Chinese medicine (TCM) has also been extensively used in the treatment of COVID-19 in China though the direct antiviral effect of TCM awaits investigation. It should be noted that the effective concentrations (generally EC50 for the reduction of viral RNA) of most previously selected drugs are in the micromolar (μM) concentration range and the selection indices reflecting drug safety leave much to be improved. Effective antivirals with good safety profile are urgently needed.

In this study, we discovered that protoporphyrin IX and verteporfin, two FDA-approved drugs that are being used in treatment of human diseases, had significant antiviral effect against SARS-CoV-2, with EC50 values for the reduction of viral RNA at nanomolar concentrations. Both drugs completely inhibited the

cytopathic effect (CPE) produced by SARS-CoV-2 infection at lower drug concentrations than that of remdesivir. The selection indices of the two drugs are 952.74 and 368.93, respectively, suggesting wide safety margins. The mechanism of the antiviral effect of protoporphyrin IX and verteporfin has been explored. The compounds interact with viral receptor ACE2 as revealed by molecular docking and might interfere with the interaction between ACE2 and viral S protein.

MATERIALS AND METHODS

Cell line, virus and compounds

African green monkey kidney Vero-E6 cell line was cultured at 37□ with 5% CO_2 in Dulbecco's modified Eagle medium (DMEM) (Gibco, Carlsbad, USA) containing 2 mmol/L L-glutamine, 50 U/mL penicillin, 100 mg/mL streptomycin, and 10% (vol/vol) fetal bovine serum (Gibco). Vero-E6 cells after SARS-CoV-2 infection were maintained with DMEM containing 2 mmol/L L-glutamine, 50 U/mL penicillin, 100 mg/mL streptomycin, and 2% (vol/vol) fetal bovine serum.

A clinical isolate of SARS-CoV-2, nCoV-SH01 (GenBank: MT121215.1) [13], was propagated in Vero-E6 cells and viral titer was determined as plaque forming units (PFU) per milliliter (mL) by CPE quantification. All the infection experiments were performed in the biosafety level-3 (BSL-3) laboratory of Fudan University.

Custom compound libraries containing 3200 small molecules were purchased from Target Mol (MA, USA). Protoporphyrin IX (CAS No.: 553-12-8), verteporfin (CAS No.: 129497-78-5) and remdesivir (CAS No. :1809249-37-3) were purchased from MedChemExpress (NJ, USA).

Cell cytotoxicity assay

The Cell Counting Kit-8 (Dojindo, Kumamoto, Japan) was used to assess cell viability according to the manufacturer's instructions. Briefly, Vero-E6 cells were dispensed into 96-well plate (1.0×10^4 cells/well), cultured in medium supplemented with the compound of different concentrations for 48 hours. After removal of the

medium, the cells were incubated with fresh serum-free medium containing 10% CCK-8 for 1 hour at 37□ and then the absorbances at 450 nm were measured using a microplate reader (Bio-Rad, Hercules, USA).

Library screening

Custom compound libraries were screened via observation of CPE. Vero-E6 cells cultured in 96-well plate (4.0 x 10^4 cells/well) were incubated with medium containing 200 PFU SARS-CoV-2/well and each compound (10 μM). Remdesivir (10 μM) served as positive control and DMSO as solvent control. CPE was observed under microscope every 24 hours for 72 hours.

Evaluation of antiviral effect of the compounds

Vero-E6 cells cultured in 96-well plate (4.0 x 10^4 cells/well) were pre-treated with the compound of a tested concentration or DMSO for 1 hour. SARS-CoV-2 (200 PFU/well) diluted in medium supplemented with the compound of the corresponding concentration was added to allow viral infection for 1 hour at 37□. The mixture was removed and cells were washed twice with PBS, followed by culture with fresh medium containing the compound of the corresponding concentration. At 48 hours post infection, culture supernatant was collected for viral RNA quantification and the cells were fixed in 4% paraformaldehyde for immunofluorescence analysis.

To evaluate the relationship between the timing of compound addition and the antiviral efficacy, Vero-E6 cells cultured in 96-well plate (4.0 x 10^4 cells/well) were treated with protoporphyrin IX (2.5 μM), verteporfin (1.25 μM) or DMSO at different timepoints relative to virus infection (Fig. 2a). Briefly, four sets of cells (I-IV) were pre-treated with the compound for 1 hour prior to virus infection. The medium was discarded and the cells were washed twice with PBS. Two sets (I, II) were then incubated with medium containing SARS-CoV-2 (200 PFU/well) and the compound for 1 hour and the other two sets (III, IV) were incubated only with the virus. After the removal of the virus and wash with PBS, set I and III were cultured with fresh

medium containing the compound while set II and IV in medium without the compound. Four more sets of cells (V-VIII) were set up similarly except the initial culture medium contains DMSO instead of the compound. At 48 hours post infection, culture supernatant was collected for viral RNA quantification and cells for immunofluorescence analysis.

For evaluation of the prevention of viral infection by the compounds, Vero-E6 cells plated in 96-well plate (4.0 x 10^4 cells/well) were pre-treated with protoporphyrin IX (2.5 μM), verteporfin (1.25 μM) or DMSO for 1 hour. The compound was removed and cells were washed with PBS twice. Subsequently, the cells were incubated with medium containing an increasing dose of SARS-CoV-2 for 1 hour. After removal of the virus and wash with PBS, cells were cultured for 48 hours for immunofluorescence analysis.

Viral RNA extraction and quantitative real time PCR (qRT-PCR)

Viral RNA in cell supernatant was extracted using TRIzol reagent (Invitrogen, Carlsbad, USA) following the manufacturer's instructions. After phenol/chloroform extraction and isopropanol precipitation, RNA was reverse transcribed using cDNA Synthesis Kit (Tiangen, Shanghai, China) according to the manufacturer's instructions. Quantitative real-time PCR (qRT-PCR) was performed in a 20 μL reaction containing SYBR Green (TaKaRa, Kusatsu, Japan) on MXP3000 cycler (Stratagene, La Jolla, USA) with the following program: initial denaturation at 95°C for 300 seconds; 40 cycles of 95°C for 15 seconds, 55°C for 20 seconds, and 72°C for 20 seconds; followed by a melt curve step. PCR primers (Genewiz, Suzhou, China) targeting SARS-CoV-2 N gene (nt608-706) were as following(forward/reverse):5'-GGGGAACTTCTCCTGCTAGAAT-3'/5'-CAGACAT TTTGCTCTCAAGCTG-3'.

Immunofluorescence analysis

To detect the viral nucleocapsid protein (N protein), anti-N polyclonal antibodies were

generated using standard immunization of Balb/C mice with recombinant N protein derived from *E. coli*. Vero-E6 cells grown in 96-well plate were fixed in 4% paraformaldehyde, permeabilized by 0.2% Triton X-100 (Thermo Fisher Scientific, Waltham, USA), blocked with 3% BSA, and stained overnight with the anti-N antibody (1:1000) at 4°C. The samples were finally incubated with Alexa Fluor donkey anti-mouse IgG 488-labeled secondary antibody (1:1000, Thermo Fisher Scientific) for 1 hour at 37°C. The nuclei were stained with DAPI (Thermo Fisher Scientific). Images were captured with fluorescence microscopy (Thermo Fisher Scientific).

Molecular docking

Cryo-electron microscopy structures of the full-length human ACE2 and a neutral amino acid transporter B^0AT1 complex with an overall resolution of 2.9 A□ have been reported [14]. The structure files were downloaded from Protein Data Bank (PDB ID: 6m18). Meanwhile, the structures of the compounds, protoporphyrin IX and verteporfin, were obtained from the EMBL-EBI and PubChem compound databases.

The receptor-ligand docking of the ACE2 protein with protoporphyrin IX or verteporfin was performed by using AutoDock 4.2.6 software and visualized with AutoDockTools 1.5.6 software (http://autodock.scripps.edu). Firstly, the ligand and receptor coordinate files were prepared respectively to include the information needed by AutoDock and the PDBQT files were created. Then the three-dimension of the grid box was set in AutoDockTools to create the grid parameter file. Afterwards, AutoGrid was used to generate the grid maps and AutoDock was run for receptor-ligand docking. After docking was completed, the results were shown in AutoDockTools, then the binding energy and receptor-ligand interactions were evaluated. The docking area was displayed in VMD 1.9.3 software (http://www.ks.uiuc.edu/Research/vmd).

Cell-cell fusion assay

Cell-cell fusion was performed as described previously [15]. Briefly, target HEK293T cells were transiently co-transfected with pCMV-eGFP and pcDNA3.1-ACE2 via

polyethylenimine (PEI). Effector HEK293T cells were generated by transfection with envelope-expressing plasmid of pCAGGS-SARS-CoV-2-S. At 24 hours post transfection, the effector cells were pre-treated with protoporphyrin IX (2.5 μM), verteporfin (1.25 μM) or DMSO for 1 hour, then the compound was removed and cells were washed with PBS twice. The target cells were quickly trypsinized and added to adherent effector cells in a 1:1 effector-to-target cell ratio. After a 4-hour cocultivation period, five fields were randomly selected in each well to count the number of fused and unfused cells under an inverted fluorescence microscope.

Statistical analysis

Data were analyzed using Prism 7 (GraphPad) and are presented as mean ± SEM. The dose response curves of viral RNA levels or cell viability *versus* the drug concentrations were plotted and evaluated by Prism 7. Statistical significance was determined using the unpaired two-tailed Student's *t* test for single variables and two-way ANOVA followed by Bonferroni posttests for multiple variables. A *P* value of <0.05 was considered statistically significant and is presented as *** ($P < 0.001$).

RESULTS

Effective inhibition of SARS-CoV-2 infection by protoporphyrin IX and verteporfin

A compound library of 3200 small molecules was screened via observation of viral CPE in Vero-E6 cells for novel antivirals that can effectively inhibit SARS-CoV-2 infection. Two compounds, protoporphyrin IX and verteporfin, showed a complete suppression of viral CPE at 1.25 μM and 0.31 μM respectively (Fig. 1b). These two compounds were subject to further analysis. At 48 hours post-infection, viral RNA level in the supernatant of the cells treated with the compound was measured using qRT-PCR, which decreased dose-dependently as compound concentration was increased. Based on the RNA level-compound concentration curve, the EC50 values of protoporphyrin IX, verteporfin and the positive control remdesivir were calculated

to be 0.23 μM, 0.03 μM, and 1.35 μM (Fig. 1a), respectively. The EC50 of remdesivir was comparable to the previous report [10]. Cell viability assay was also performed and a viability-compound concentration curve was drawn (Fig. 1a), from which the CC50 values of protoporphyrin IX, verteporfin and remdesivir were determined to be 219.13 μM, 10.33 μM, and 303.23 μM, respectively. The selection indices (S.I.) for the three compounds could thus be calculated as 952.74, 368.93, and 224.61, respectively. Viral N protein expression in infected Vero-E6 cells was assessed by immunofluorescence. The data revealed the complete inhibition of N protein expression by protoporphyrin IX, verteporfin and remdesivir at 1.25 μM, 0.31 μM, and 6.25 μM, respectively (Fig. 1b). The results indicate that protoporphyrin IX and verteporfin strongly inhibit the infection of SARS-CoV-2 at nanomolar concentrations and have a wide safety range *in vitro*.

Effects of treatment timing on protoporphyrin IX and verteporfin's inhibition of SARS-CoV-2 infection

We next analyzed the relationship between the antiviral effect and treatment timing of protoporphyrin IX and verteporfin. As shown in Fig. 2a, Vero-E6 cells were treated with protoporphyrin IX, verteporfin or the solvent DMSO before viral infection, during viral entry and after viral entry. A total of 8 treatment groups were set up for each compound (group I-VIII). Based on the previous results, we selected the compound concentrations of 2.5 μM and 1.25 μM for protoporphyrin IX and verteporfin, respectively. At 48 hours post infection, viral RNA level in the cell supernatant was quantified with qRT-PCR. The results showed that viral RNA levels of all the compound-treated groups (group I-VII of each compound in Fig. 2b, 2c) were significantly lower than that of the DMSO-treated group (group VIII in Fig. 2b, 2c). Importantly, pre-treatment alone resulted in the complete inhibition of SARS-CoV-2 infection (group IV in Fig. 2b, 2c). In addition, treatment of cells with protoporphyrin IX or verteporfin after viral infection also inhibited viral RNA production, albeit to different extent (group VII in Fig. 2b, 2c). The results of immunofluorescence analysis on intracellular viral N protein were consistent with

those of viral RNA measurement (Fig. 2d). Collectively, the results indicate that protoporphyrin IX and verteporfin can prevent SARS-CoV-2 infection as well as suppress established SARS-CoV-2 infection.

The preventive effect was further tested by the pre-treatment of cells with either compound at a constant concentration and later infection with an increasing virus titer (Fig. 3a). As shown in Fig. 3b, no viral N protein expression was detected in protoporphyrin IX or verteporfin pre-treated cells even if the inoculated viral titer was raised by 16 folds (200 PFU - 3200 PFU).

Protoporphyrin IX and verteporfin may interact with human ACE2 protein

Protoporphyrin IX and verteporfin share a same porphyrin-ring structure (Fig. 4a) and thus likely act through a common antiviral mechanism. One possibility prompted by the pre-treatment/preventive results was the saturation or modification of an essential cellular factor(s) required for viral infection. We thus investigated by molecular docking analysis whether ACE2, the viral receptor, might be the target of the compounds. The ACE2 peptidase domain (PD) from the human ACE2-B^0AT1 complex (PDB ID: 6m18) [14] was used for docking with protoporphyrin IX and verteporfin (Fig. 4a). The result with the highest ranking is exhibited in Fig. 4b, which represents the molecular model of protoporphyrin IX or verteporfin binding to PD. Protoporphyrin IX is located in the shallow-pocket-like space in the PD, with a binding energy of -5.60 kcal/mol. Similar result was obtained from the docking of verteporfin with PD (with a binding energy of -5.35 kcal/mol). Fig. 4c provides a view of the interaction of protoporphyrin IX or verteporfin with ACE2 PD residues. In the model, 25 residues of the PD interacted with protoporphyrin IX, in which the benzene ring of Phe^{40} interacted closely with the porphyrin-ring of protoporphyrin IX, the Trp^{69} formed aromatic H-bonds with the porphyrin-ring, Asp^{350} and Asp^{382} formed H-bonds with the compound. The other residues involved in the interaction with protoporphyrin IX included Ser^{43}, Ser^{44}, Ser^{47}, Asn^{51}, Gly^{66}, Ser^{70}, Leu^{73}, Thr^{347}, Ala^{348}, Trp^{349}, Leu^{351}, Gly^{352}, Phe^{356}, His^{378}, Ile^{379}, Tyr^{385}, Phe^{390}, Leu^{391}, Arg^{393},

Asn[394] and His[401]. Similar results were observed in the interaction between verteporfin and PD, except that Asn[51] formed additional H-bonds with the benzazole-like structure of verteporfin. Many of these PD residues are located in the region that interacts with SARS-CoV-2 S protein receptor binding domain (RBD), especially Phe[40], Ser[43], Ser[44], Trp[349]- Gly[352] and Phe[356], which are very close to the key residues (Tyr[41], Gln[42], Lys[353] and Arg[357]) that interact with the RBD[14]. The results suggest that protoporphyrin IX and verteporfin might interact with ACE2.

Protoporphyrin IX and verteporfin block cell-cell fusion mediated by SARS-CoV-2 S protein and ACE2

We tested the activity of protoporphyrin IX and verteporfin in interference with ACE2-S interaction using a cell-cell fusion assay system. HEK293T cells that express SARS-CoV-2 S protein served as the effector cells and those co-expressing human ACE2 and eGFP as the target cells (Fig. 4d). The target cells were pre-treated with protoporphyrin IX (2.5 μM), verteporfin (1.25 μM) or DMSO for 1 hour. After removal of the drug, the target and effector cells were co-cultured at 37□ for 4 hours. Fused cells with larger cell size than normal cells were observed in the DMSO-treated group but barely in the protoporphyrin IX or verteporfin-treated group. The results indicate that protoporphyrin IX and verteporfin may block the cell-cell fusion mediated by the interaction of ACE2 and viral S protein.

DISCUSSION

Protoporphyrin IX and verteporfin have been approved and used in the treatment of human diseases. Protoporphyrin IX is the final intermediate in the protoporphyrin IX iron complex (heme) biosynthetic pathway [16]. Heme is an important cofactor for oxygen transfer and oxygen storage[17] and is a constituent of hemoproteins which play a variety of roles in cellular metabolism[18]. The light-activable photodynamic effect of protoporphyrin IX was used for cancer diagnosis[19] and approved by FDA for treatment of bronchial and esophageal cancers and early malignant lesions of the skin,

bladder, breast, stomach, and oral cavity[20, 21]. Verteporfin was approved for the treatment of age-related macular degeneration [22]. The potential of verteporfin for the treatment of cancers, such as prostatic cancer, breast cancer, and pancreatic ductal adenocarcinoma has been investigated [23]. Verteporfin also has been reported to inhibit autophagy at an early stage by suppressing autophagosome formation [24]. Our study discovered potent antiviral effects of protoporphyrin IX and verteporfin on SARS-CoV-2 infection. The effective concentrations of these drugs are in the nanomolar concentration range. In addition, the selection indices of both drugs are greater than 200, indicating better safety margins. Nevertheless, this study was performed with Vero-E6 cell culture system. The antiviral efficacy of protoporphyrin IX and verteporfin *in vivo* will need clinical evaluation.

Both protoporphyrin IX and verteporfin have a porphyrin ring structure formed by four pyrrole rings. It can be deduced that they share a similar mechanism of antiviral action. In the experiment when either drug was added prior to viral infection, viral RNA production was inhibited even if the relevant drug was not added in the later virus infection and post-infection stages (group IV in Fig. 2b, 2c). Furthermore, increasing viral titer did not relieve the inhibition of the drugs added before viral infection (Fig. 3b). A logical hypothesis is that both drugs act by inhibiting an early step in viral infection. Structural simulation by molecular docking supports the binding of both drugs to viral receptor ACE2. Several residues on ACE2 predicted to interact with the drugs are very close to the key residues that interact with the RBD of viral S protein. Based on the molecular docking and experimental data, both drugs are likely to bind ACE2, which might interfere with the interaction between ACE2 and the RBD and impairs viral entry. The mechanism was also supported by the blocking effect of both drugs on the cell-cell fusion mediated by the interaction of ACE2 and viral S protein. More detailed mechanism warrants further study. The study suggests a new venue for the development small molecule-based entry inhibitor against SARS-CoV-2.

On the other hand, protoporphyrin IX and verteporfin were able to inhibit viral RNA production when they were added after viral infection (group VII in Fig. 2b, 2c). Although it is possible that the drugs might inhibit the infection of progeny viruses and prevent virus spreading, the absence of N protein expression in post-infection verteporfin-treated cells suggests that there may also be intracellular antiviral mechanism. Whether the drugs stimulate an antiviral innate immune response also needs exploration.

In conclusion, our study demonstrate the potent antiviral activities of protoporphyrin IX and verteporfin against SARS-CoV-2 infection and also shed new light on the development of novel antivirals against SARS-CoV-2.

ACKNOWLEDGMENTS

The study was supported by the National Science and Technology Major Project (NSTMP) for the Prevention and Treatment of Infectious Diseases (2018ZX10734401, 2018ZX10301208), NSTMP for the Development of Novel Drugs (2019ZX09721001), and Project of Novel Coronavirus Research of Fudan University.

AUTHOR CONTRIBUTIONS

Youhua Xie, Di Qu and Qing Deng drafted the manuscript. Youhua Xie, Di Qu and Qiang Deng designed the project. The majority of the experiments and data analysis were performed by Chenjian Gu, Yang Wu and Huimin Guo. The other authors participated in the data analysis and manuscript revision. All the authors have approved the manuscript.

Competing interests: The authors declare no competing interests.

REFERENCES

1 Holshue ML, DeBolt C, Lindquist S *et al.* First Case of 2019 Novel Coronavirus in the United States. *New England Journal of Medicine* 2020; **382**:929-936.
2 Elfiky AA. Ribavirin, Remdesivir, Sofosbuvir, Galidesivir, and Tenofovir against SARS-CoV-2 RNA dependent RNA polymerase (RdRp): A molecular docking study. *Life Sciences* 2020; **253**:117592.
3 Grein J, Ohmagari N, Shin D *et al.* Compassionate Use of Remdesivir for Patients with Severe Covid-19. *New England Journal of Medicine* 2020.
4 Cao B, Wang Y, Wen D *et al*. A Trial of Lopinavir–Ritonavir in Adults Hospitalized with Severe Covid-19. *New England Journal of Medicine* 2020.
5 Costanzo M, De Giglio MAR, Roviello GN. SARS-CoV-2: Recent Reports on Antiviral Therapies Based on Lopinavir/Ritonavir, Darunavir/Umifenovir, Hydroxychloroquine, Remdesivir, Favipiravir and Other Drugs for the Treatment of the New Coronavirus. *Curr Med Chem* 2020.
6 Tu YF, Chien CS, Yarmishyn AA *et al*. A Review of SARS-CoV-2 and the Ongoing Clinical Trials. *Int J Mol Sci* 2020; **21**.
7 Caly L, Druce JD, Catton MG, Jans DA, Wagstaff KM. The FDA-approved drug ivermectin inhibits the replication of SARS-CoV-2 in vitro. *Antiviral Res* 2020; **178**:104787.
8 Gautret P, Lagier JC, Parola P *et al*. Hydroxychloroquine and azithromycin as a treatment of COVID-19: results of an open-label non-randomized clinical trial. *Int J Antimicrob Agents* 2020:105949.
9 Cortegiani A, Ingoglia G, Ippolito M, Giarratano A, Einav S. A systematic review on the efficacy and safety of chloroquine for the treatment of COVID-19. *J Crit Care* 2020.
10 Wang M, Cao R, Zhang L *et al*. Remdesivir and chloroquine effectively inhibit the recently emerged novel coronavirus (2019-nCoV) in vitro. *Cell Res* 2020; **30**:269-271.
11 Suranagi UD, Rehan HS, Goyal N. Hydroxychloroquine for the management of COVID-19: Hope or Hype? A Systematic review of the current evidence. *medRxiv* 2020:2020.2004.2016.20068205.
12 Magagnoli J, Narendran S, Pereira F *et al*. Outcomes of hydroxychloroquine usage in United States veterans hospitalized with Covid-19. *medRxiv* 2020:2020.2004.2016.20065920.
13 Rong Z, Zhigang Y, Yuyan W *et al*. Isolation of a 2019 novel coronavirus strain from a coronavirus disease 19 patient in Shanghai. *JOURNAL OF MICROBES AND INFECTIONS* 2020; **15**:111-121.
14 Yan R, Zhang Y, Li Y, Xia L, Guo Y, Zhou Q. Structural basis for the recognition of SARS-CoV-2 by full-length human ACE2. *Science* 2020; **367**:1444-1448.
15 Xia S, Liu M, Wang C *et al.* Inhibition of SARS-CoV-2 (previously 2019-nCoV) infection by a highly potent pan-coronavirus fusion inhibitor targeting its spike protein that harbors a high capacity to mediate membrane fusion. *Cell Res* 2020; **30**:343-355.
16 Sachar M, Anderson KE, Ma X. Protoporphyrin IX: the Good, the Bad, and the Ugly. *J Pharmacol Exp Ther* 2016; **356**:267-275.
17 Shimizu T, Lengalova A, Martinek V, Martinkova M. Heme: emergent roles of heme in signal transduction, functional regulation and as catalytic centres. *Chem Soc Rev* 2019; **48**:5624-5657.
18 Smith LJ, Kahraman A, Thornton JM. Heme proteins--diversity in structural characteristics, function, and folding. *Proteins* 2010; **78**:2349-2368.
19 Ishizuka M, Abe F, Sano Y *et al*. Novel development of 5-aminolevurinic acid (ALA) in cancer diagnoses and therapy. *Int Immunopharmacol* 2011; **11**:358-365.
20 Pass HI. Photodynamic therapy in oncology: mechanisms and clinical use. *J Natl Cancer Inst* 1993; **85**:443-456.
21 Oleinick NL, Evans HH. The photobiology of photodynamic therapy: cellular targets and

mechanisms. *Radiat Res* 1998; **150**:S146-156.
22 Schmidt-Erfurth U, Hasan T. Mechanisms of action of photodynamic therapy with verteporfin for the treatment of age-related macular degeneration. *Surv Ophthalmol* 2000; **45**:195-214.
23 Pellosi DS, Calori IR, de Paula LB, Hioka N, Quaglia F, Tedesco AC. Multifunctional theranostic Pluronic mixed micelles improve targeted photoactivity of Verteporfin in cancer cells. *Mater Sci Eng C Mater Biol Appl* 2017; **71**:1-9.
24 Donohue E, Tovey A, Vogl AW *et al.* Inhibition of autophagosome formation by the benzoporphyrin derivative verteporfin. *J Biol Chem* 2011; **286**:7290-7300.

Figure legends

Figure 1 Effective inhibition of SARS-CoV-2 infection by protoporphyrin IX and verteporfin

a. Antiviral effect and cell cytotoxicity of protoporphyrin IX and verteporfin. The viral RNA production in the supernatant of infected Vero-E6 cells was quantified with qRT-PCR. The value at each compound concentration was presented relative to that at zero compound concentration that was set as 100% (blue). The percentage of reduction in viable cells at different compound concentration (red) was measured using the CCK8 assay. The value at each compound concentration was calculated using the formula, 100-Value (compound concentration)/Value (zero compound concentration). EC50, concentration for 50% of maximal effect; CC50, concentration for 50% of maximal cytotoxic effect; S.I., selection index. Data from three independent experiments were analyzed. **b.** Immunofluorescence of intracellular viral N protein. Intracellular expression of N protein was assessed by staining of infected Vero-E6 cells with the polyclonal anti-N antibody (1:1000 dilution, green). Nuclei were stained with DAPI. CPE was shown in bright field.

Figure 2 Effects of treatment timing of protoporphyrin IX and verteporfin on SARS-CoV-2 infection

a. Schematic presentation of treatment timing of protoporphyrin IX and verteporfin. Briefly, Vero-E6 cells were treated with protoporphyrin IX, verteporfin or the solvent DMSO before viral infection, during viral entry and after viral entry. A total of 8 treatment groups (I-VIII) for each compound were set up. **b.** Antiviral effect of different treatment timing. Viral RNA level in the supernatant of infected Vero-E6 cells was quantified with qRT-PCR. The values of group I to VII were presented relative to that of group VIII which was set as 100%, respectively. Statistical significance was determined using the unpaired two-tailed Student's *t* test. *** $P < 0.001$. Data from three independent experiments were analyzed. **c**. Immunofluorescence of intracellular viral N protein. Intracellular expression of N

protein of different treatment timing was assessed by staining of infected Vero-E6 cells with the polyclonal anti-N antibody (1:1000 dilution, green). Nuclei were stained with DAPI.

Figure 3 Protoporphyrin IX and verteporfin prevent SARS-CoV-2 infection

a. Schematic presentation of treatment design. Briefly, Vero-E6 cells were pre-treated with protoporphyrin IX, verteporfin or the solvent DMSO before viral infection for 1 hour, then the drugs were removed and the cells were washed and infected with an increasing titer of SARS-CoV-2. **b.** CPE of the cells with the different treatment. **c**. Immunofluorescence of intracellular viral N protein. Intracellular expression of N protein of different treatment was assessed by staining of infected Vero-E6 cells with the polyclonal anti-N antibody (1:1000 dilution, green). Nuclei were stained with DAPI.

Figure 4 Molecular docking of protoporphyrin IX and verteporfin with human ACE2 protein

a. Structures of protoporphyrin IX and verteporfin. **b.** Docking of ACE2 peptidase domain (PD) with protoporphyrin IX (blue) and verteporfin (pink). The 3D structure of PD is from cryo-electron microscopy structure of the ACE2-B^0AT1 complex (PDB ID: 6m18). The surface of PD is shown. **c.** Interactions of protoporphyrin IX (upper) or verteporfin (bottom) with ACE2 residues. **d**. Blocking effect on ACE2 and SARS-CoV-2 S-mediated cell-cell fusion by protoporphyrin IX and verteporfin. The inhibitory value of protoporphyrin IX or verteporfin-treated group was presented relative to that of the DMSO-treated group which was set as 100%, respectively. Statistical significance was determined using the unpaired two-tailed Student's t test. *** $P < 0.001$.

Figure 1

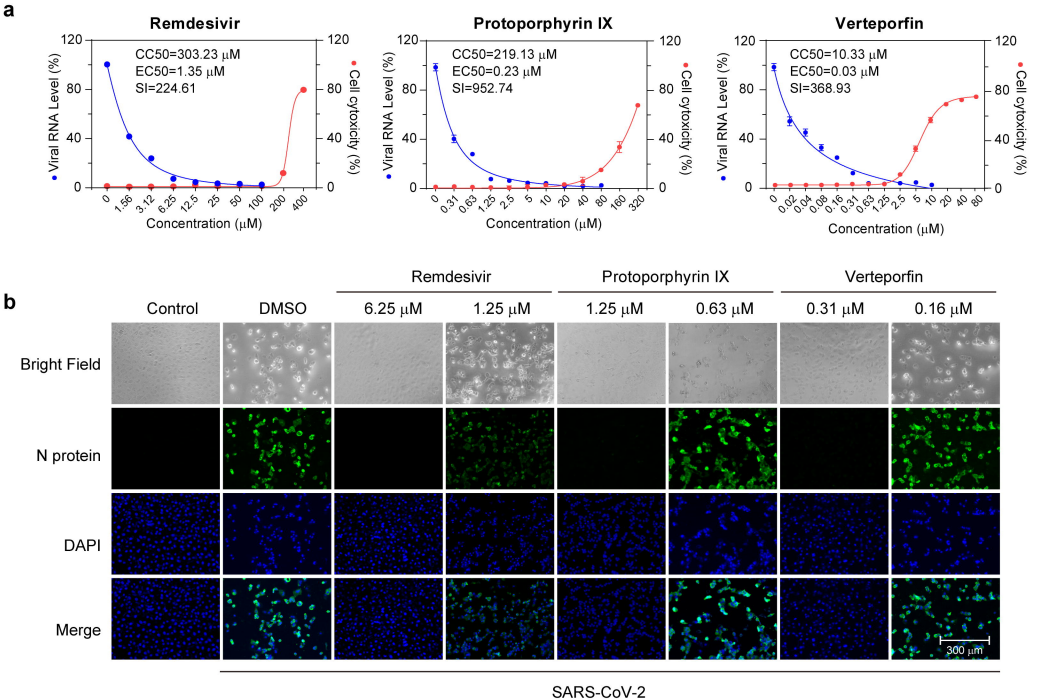
a
Remdesivir
CC50=303.23 μM
EC50=1.35 μM
SI=224.61
Protoporphyrin IX
CC50=219.13 μM
EC50=0.23 μM
SI=952.74
Verteporfin
CC50=10.33 μM
EC50=0.03 μM
SI=368.93
Viral RNA Level (%)
Cell cytoxicity (%)
Concentration (μM)
b
Control
DMSO
Remdesivir
6.25 μM
1.25 μM
Protoporphyrin IX
1.25 μM
0.63 μM
Verteporfin
0.31 μM
0.16 μM
Bright Field
N protein
DAPI
Merge
300 μm
SARS-CoV-2

Figure 2

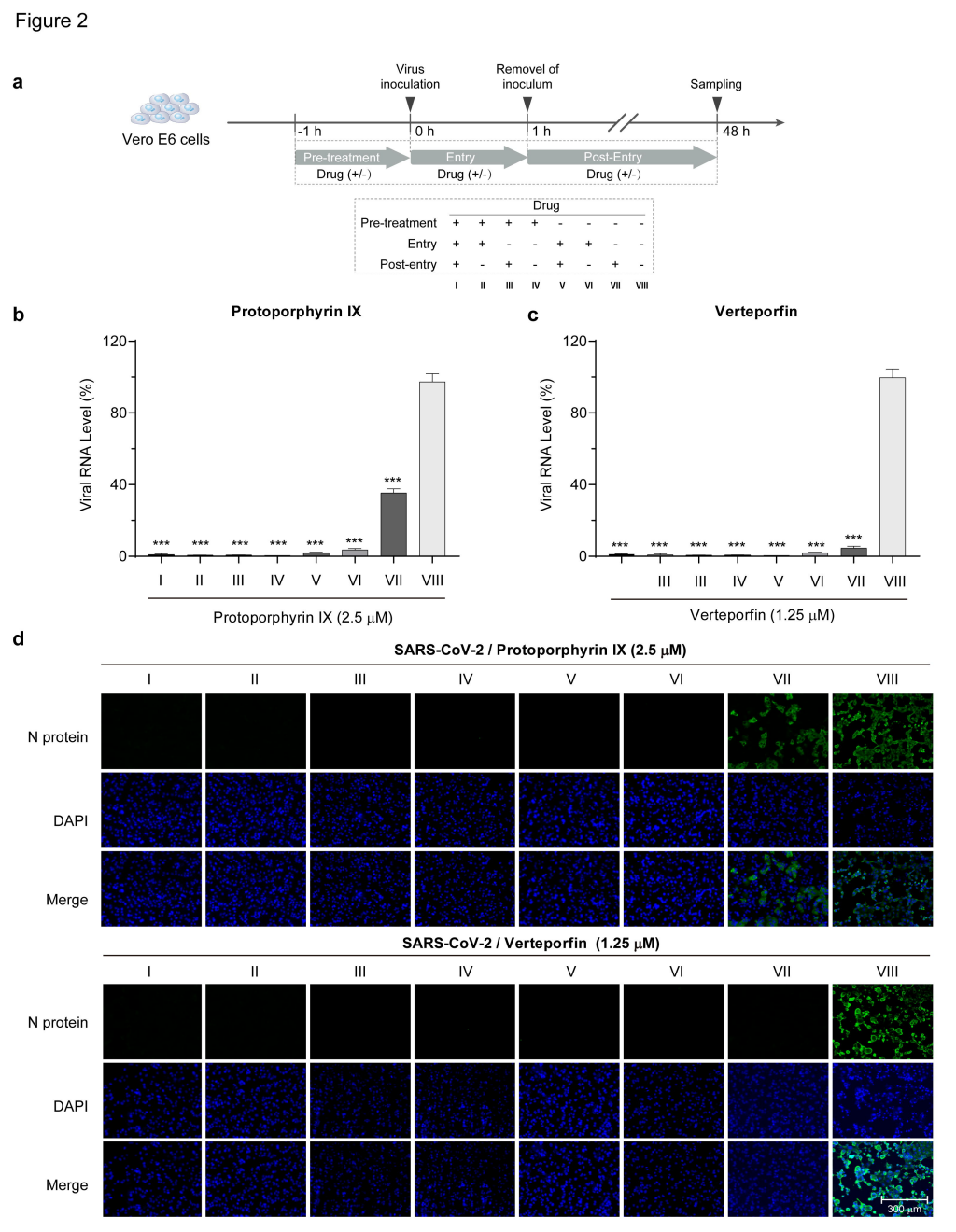
a
Vero E6 cells
Virus inoculation
Removel of inoculum
Sampling
-1 h
0 h
1 h
48 h
Pre-treatment
Drug (+/-)
Entry
Drug (+/-)
Post-Entry
Drug (+/-)
Drug
Pre-treatment + + + + - - - -
Entry + + - - + + - -
Post-entry + - + - + - + -
I II III IV V VI VII VIII
b
Protoporphyrin IX
Viral RNA Level (%)
120
80
40
0
***
I II III IV V VI VII VIII
Protoporphyrin IX (2.5 μM)
c
Verteporfin
Viral RNA Level (%)
120
80
40
0
***
III III IV V VI VII VIII
Verteporfin (1.25 μM)
d
SARS-CoV-2 / Protoporphyrin IX (2.5 μM)
I II III IV V VI VII VIII
N protein
DAPI
Merge
SARS-CoV-2 / Verteporfin (1.25 μM)
I II III IV V VI VII VIII
N protein
DAPI
Merge
300 μm

Figure 3

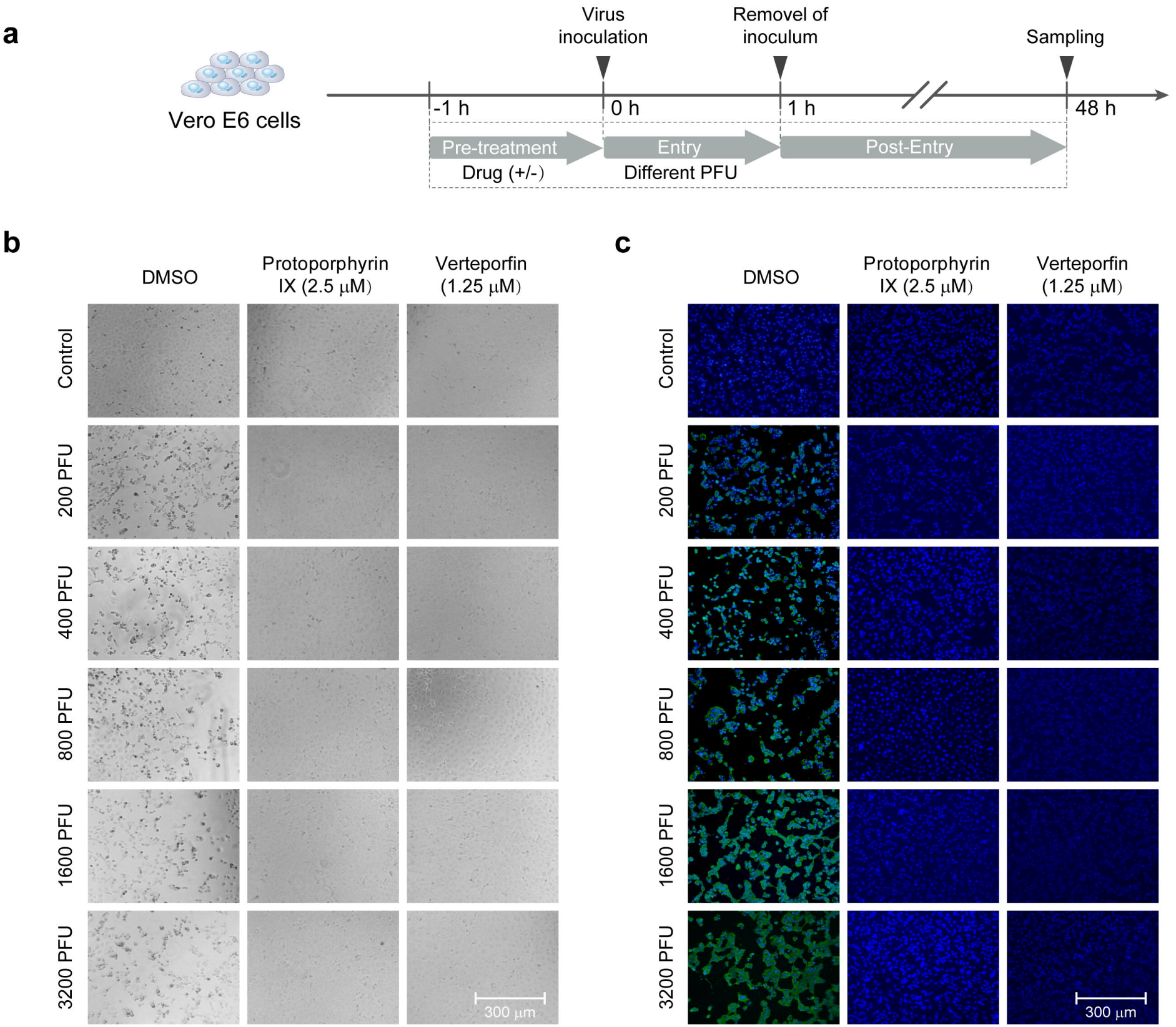
a
Vero E6 cells
Virus inoculation
Removel of inoculum
Sampling
-1 h
0 h
1 h
48 h
Pre-treatment
Drug (+/-)
Entry
Different PFU
Post-Entry
b
DMSO
Protoporphyrin IX (2.5 μM)
Verteporfin (1.25 μM)
Control
200 PFU
400 PFU
800 PFU
1600 PFU
3200 PFU
300 μm
c
DMSO
Protoporphyrin IX (2.5 μM)
Verteporfin (1.25 μM)
Control
200 PFU
400 PFU
800 PFU
1600 PFU
3200 PFU
300 μm

Figure 4

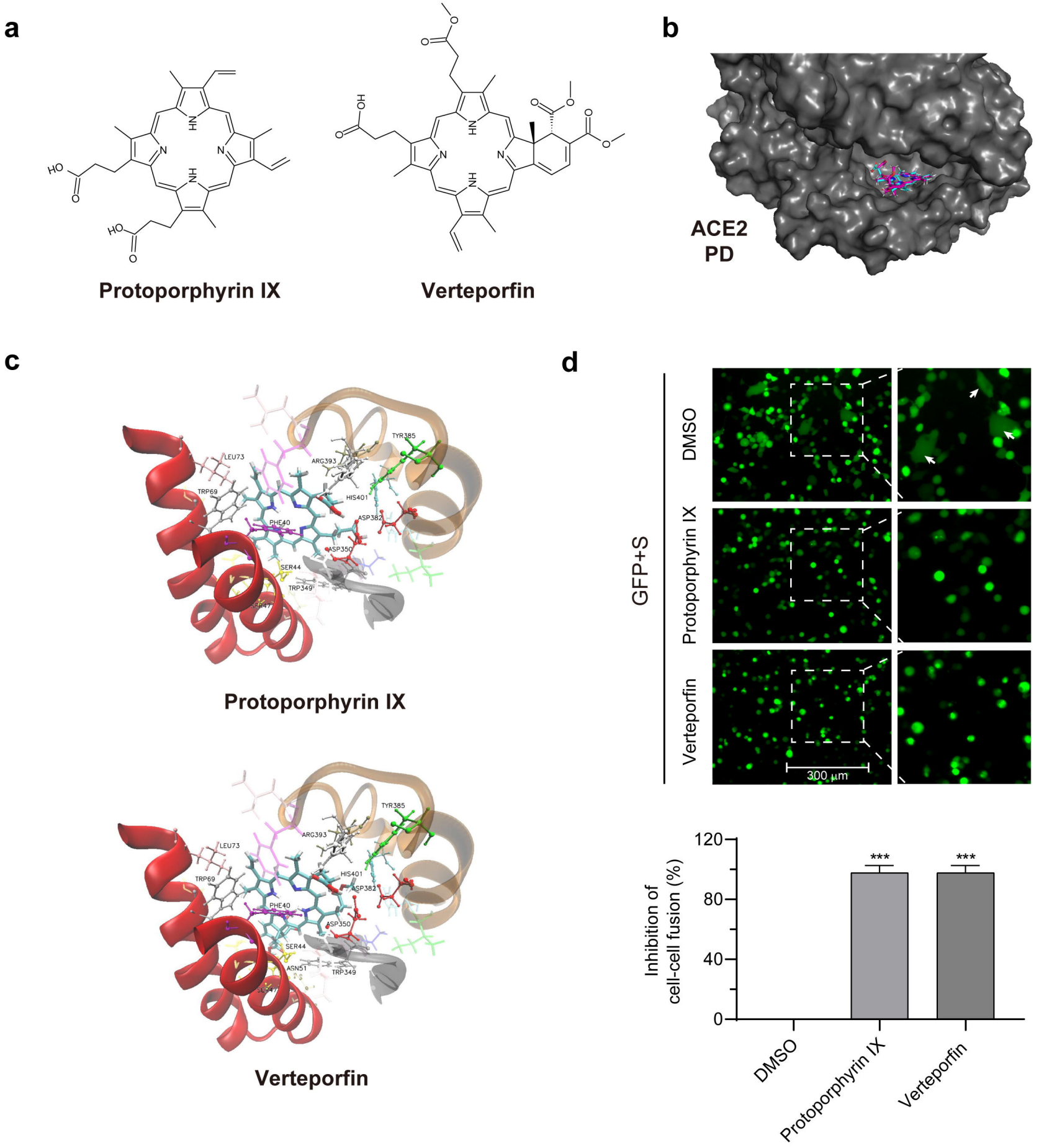
a
Protoporphyrin IX
Verteporfin
b
ACE2
PD
c
LEU73
TYR385
ARG393
TRP69
HIS401
PHE40
ASP382
ASP350
SER44
TRP349
Protoporphyrin IX
LEU73
TYR385
ARG393
TRP69
HIS401
PHE40
ASP382
ASP350
SER44
ASN51
TRP349
Verteporfin
d
GFP+S
DMSO
Protoporphyrin IX
Verteporfin
300 μm
Inhibition of cell-cell fusion (%)
120
80
40
0
***
***
DMSO
Protoporphyrin IX
Verteporfin